J. Nonlinear Funct. Anal. 2026 (2026) 10 https://doi.org/10.23952/jnfa.2026.10

MATHRES Journal of Nonlinear Functional Analysis
Available online at http://jnfa.mathres.org

CONVERGENCE OF LOCAL MULTIGRID FOR HIGH-ORDER ADAPTIVE FEM IN 3D ELASTICITY PROBLEMS

LIPING ZHOU, YINQIN LIN*

College of Science, Hunan University of Science and Engineering, Yongzhou 425199, China

Abstract. For the high-order finite element discretization system of three-dimensional elasticity problems, a local multigrid (LMG) method based on bisection grids is proposed. By decomposing the high-order finite element space into a "high-frequency" component and a linear element space, and leveraging the properties of bisection grids and interpolation operators, the stability of this space decomposition and the validity of the strong Cauchy-Schwarz inequality are proven. Consequently, the uniform convergence of the LMG algorithm is established. Numerical experiments are provided to verify the correctness of the theoretical results.

Keywords. Elasticity problems; Finite element discretization system; Local multigrid; Stability of space decomposition.

2020 MSC. 65N30, 35J20.

1. INTRODUCTION

The finite element method (FEM) is a crucial numerical method for solving three-dimensional elasticity problems [11]. However, due to the complexity of real-world applications, conventional finite elements—even higher-order elements—do not always guarantee improved accuracy. An effective solution lies in adaptive finite element methods (AFEM), which dynamically adjust mesh distribution or increase element order based on solution behavior. This strategy effectively mitigates the issue of excessive degrees of freedom caused by uniform refinement, achieving optimal computational accuracy with minimal computational cost. Today, AFEM has been widely adopted in modern scientific and engineering computations, emerging as one of the most powerful numerical techniques for addressing challenges such as non-smooth domains, discontinuous material properties, and stress concentrations [2, 3, 13, 15].

The solver module constitutes one of the primary factors determining the overall efficiency in adaptive finite element analysis [4, 5, 8, 9, 12, 14, 16–18]. Developing fast algorithms for

*Corresponding author.
E-mail address: lpz@huse.edu.cn (L. Zhou), yqlin@huse.edu.cn (Y. Lin).
Received October 10, 2025; Accepted December 20, 2025.

solving algebraically discretized systems on adaptive meshes is therefore imperative. Adaptive mesh refinement generates a sequence of nested grids, where direct solution methods would fail to preserve inter-level solution information. The multigrid (MG) method emerges as the most effective approach for such hierarchical systems. However, conventional multigrid implementations apply both pre-smoothing and post-smoothing operators globally across the entire computational domain. This leads to computational workloads that scale prohibitively with increasing adaptive refinement levels.

The recently developed locally relaxed multigrid method (LMG) [4, 5, 8, 12, 17] has demonstrated superior computational efficiency in adaptive finite element analysis. However, existing methods primarily focus on scalar elliptic equations, with limited research extending to systems of equations, particularly in elastomechanics problems. Currently, the widely adopted adaptive approach in computations utilizes Zienkiewicz-Zhu (Z-Z) type a posteriori error estimators [16]. While this adaptive method guarantees convergence, it fails to achieve optimal performance. Most recently, Reference [9] proposed an adaptive finite element method with proven convergence and quasi-optimal computational complexity for two-dimensional elastomechanics problems, along with an enhanced LMG method exhibiting improved computational efficiency and robustness. However, the three-dimensional case remains unexplored and warrants further investigation.

This paper extends the algorithmic framework and analysis methodology from [10] to the numerical solution of three-dimensional elasticity problems, developing an adaptive p-order finite element method that eliminates the need for both oscillation term marking and the "inner node" property requirement for refined elements. For solving the p-order finite element equations on adaptively refined meshes, we propose a LMG method that implements the following computational strategy: (1) performing multiple Gauss-Seidel smoothing iterations on the p-order system to dampen high-frequency error components, followed by (2) localized relaxation iterations on the corresponding linear element subspaces at each hierarchical level. Numerical experiments demonstrate that the proposed adaptive scheme maintains uniform convergence and achieves quasi-optimal computational complexity for both linear and hierarchical quadratic element cases, the accompanying LMG solver exhibits enhanced computational efficiency and improved robustness. A key innovation lies in employing hierarchical basis functions, which enables direct extraction of the linear element matrix from the p-order discretization matrix. This approach circumvents the expensive generation of mesh transformation matrices, resulting in significant CPU time savings and substantially improved computational efficiency.

2. Adaptive Finite Element Methods for Elasticity Problems

In this paper, we focus exclusively on quadratic adaptive finite element equations for three-dimensional elasticity problems, while similar conclusions can be drawn for higher-order finite element equations.

2.1. **Model problem and quadratic finite element equation.**

Consider three-dimensional elasticity problem with Dirichlet boundary conditions as follows

$$\mathbf{L}u =: -\mathscr{L}^T(\partial_x,\partial_y,\partial_z)D\mathscr{L}(\partial_x,\partial_y,\partial_z)u = f,\ (x,y,z)\in\Omega, \tag{2.1}$$

$$u = g,\ (x,y,z)\in\partial\Omega, \tag{2.2}$$

where $\Omega \subset \mathbb{R}^3$ is a bounded Lipschitz polyhedral domain. u is a displacement vector, f and g are an external force and given vector functions, respectively, $n = (n_x, n_y, n_z)^T$ is a unit normal vector defined on the boundary $\partial\Omega$, the operators $\mathscr{L}(a,b,c)$ and D are defined by the following expressions

$$\mathscr{L}(a,b,c) = \begin{pmatrix} a & 0 & 0 \\ 0 & b & 0 \\ 0 & 0 & c \\ b & a & 0 \\ 0 & c & b \\ c & 0 & a \end{pmatrix}, \; D = \begin{pmatrix} \lambda+2\mu & \lambda & \lambda & 0 & 0 & 0 \\ \lambda & \lambda+2\mu & \lambda & 0 & 0 & 0 \\ \lambda & \lambda & \lambda+2\mu & 0 & 0 & 0 \\ 0 & 0 & 0 & \mu & 0 & 0 \\ 0 & 0 & 0 & 0 & \mu & 0 \\ 0 & 0 & 0 & 0 & 0 & \mu \end{pmatrix},$$

where λ and μ are the Lamé constants, which can be expressed in terms of the elastic modulus E and Poisson's ratio ν as follows

$$\lambda = \frac{E\nu}{(1+\nu)(1-2\nu)}, \; \mu = \frac{E}{2(1+\nu)}. \tag{2.3}$$

Define the following spaces on the domain Ω

$$H_g^1(\Omega) = \{u \in H^1(\Omega) : u|_{\partial\Omega} = g\}, \; H_0^1(\Omega) = \{u \in H^1(\Omega) : u|_{\partial\Omega} = 0\}.$$

Using the above spaces, the continuous variational formulation [6] of the model problem (2.1)-(2.2) is: For given $f, g \in L^2(\Omega)$, find $u \in H_g^1(\Omega)$ such that

$$a(u,v) = F(v), \; \forall \, v \; \in H_0^1(\Omega), \tag{2.4}$$

where

$$a(u,v) = \int_\Omega (\mathscr{L}(\partial_x, \partial_y, \partial_z)v)^T D \mathscr{L}(\partial_x, \partial_y, \partial_z) u dx, \tag{2.5}$$

$$F(v) = \int_\Omega f \cdot v dx. \tag{2.6}$$

The bilinear form $a(\cdot,\cdot)$ in the variational problem (2.4) satisfies the following properties [6]: For any $u, v \in H_g^1(\Omega)$, there holds

$$(1)\text{The boundedness:} \;\; a(u,v) \lesssim (\lambda+\mu)\|u\|_1\|v\|_1, \tag{2.7}$$

$$(2)\text{The coercivity:} \; a(u,u) \gtrsim \mu\|u\|_1^2. \tag{2.8}$$

Using (2.7) and (2.8), we can prove that the variational problem (2.4) is well-posed. From the coercivity property and the definition of the bilinear form, we conclude that $a(u,u)$ is symmetric positive definite. Therefore, for any $u \in H_g^1(\Omega)$, we can introduce the following energy norm.

$$\|u\|_{A,\Omega} = (a(u,u))^{\frac{1}{2}}.$$

Let $\mathscr{T}$ be a conforming triangular mesh partition of the domain $\Omega \subset \mathbb{R}^3$. We define the p-th order finite element space on this mesh as follows.

$$\mathbb{V}(\mathscr{P}_p, \mathscr{T}) = \{v_{\mathscr{T}} \in C(\overline{\Omega}) : v_{\mathscr{T}}|_\tau \in (P_p(\tau))^3, \forall \tau \in \mathscr{T}, v_{\mathscr{T}}|_{\partial\Omega} = g\}, \tag{2.9}$$

$$\mathbb{V}_0(\mathscr{P}_p, \mathscr{T}) = \{v_{\mathscr{T}} \in C(\overline{\Omega}) : v_{\mathscr{T}}|_\tau \in (P_p(\tau))^3, \forall \tau \in \mathscr{T}, v_{\mathscr{T}}|_{\partial\Omega} = 0\}, \tag{2.10}$$

where $P_p(\tau)$denotes the space of p-th degree polynomials on τ.

Let $M := \dim(\mathbb{V}(\mathscr{P}_p, \mathscr{T})) = 3n$, where n denotes the number of interpolation nodes in $\mathbb{V}(\mathscr{P}_p, \mathscr{T})$ with all three displacement degrees of freedom unconstrained. Let Φ_l be the p-th order finite element basis function corresponding to the l-th node ($l = 1, \cdots, n$) on mesh $\mathscr{T}$. Then the basis functions of the space $\mathbb{V}(\mathscr{P}_p, \mathscr{T})$ are given by

$$\Phi_{3l-2} = \begin{pmatrix} \phi_l \\ 0 \\ 0 \end{pmatrix}, \ \Phi_{3l-1} = \begin{pmatrix} 0 \\ \phi_l \\ 0 \end{pmatrix}, \ \Phi_{3l} = \begin{pmatrix} 0 \\ 0 \\ \phi_l \end{pmatrix}. \tag{2.11}$$

The discrete variational formulation of problem (2.4) reads: Find $u_{\mathscr{T}} \in \mathbb{V}(\mathscr{P}_p, \mathscr{T})$ such that

$$a(u_{\mathscr{T}}, v_{\mathscr{T}}) = F(v_{\mathscr{T}}), \ \forall \, v_{\mathscr{T}} \in \mathbb{V}_0(\mathscr{P}_p, \mathscr{T}). \tag{2.12}$$

Let $\mathscr{T}_0$ be a given initial mesh. Then the AFEM for solving the variational problem (2.12) from the i-th adaptively refined mesh $\widetilde{\mathscr{T}_i}$ (with $\widetilde{\mathscr{T}_0} := \mathscr{T}_0$) to the $(i+1)$-th adaptively refined mesh $\widetilde{\mathscr{T}_{i+1}}$ consists of the following steps

Algorithm 2.1. *Let $\widetilde{\mathscr{T}} := \widetilde{\mathscr{T}_i}$ and $\widetilde{u} := \widetilde{u}_i$ denote the finite element solution on $\widetilde{\mathscr{T}}$. Then the AFEM procedure (see [9, 10]) for generating the adaptively refined mesh $\widetilde{\mathscr{T}_{i+1}}$ and the corresponding finite element solution $\widetilde{u}_{i+1}$ consists of the following steps.*

(1) Compute the error indicator : $\eta^2_{\widetilde{\mathscr{T}}}(\widetilde{u}, \tau), \forall \tau \in \widetilde{\mathscr{T}}$.
(2) Determine the set of elements to be refined: $\mathscr{M}_{\widetilde{\mathscr{T}}}$.
(3) Generate the refined mesh using the bisection method: $\widetilde{\mathscr{T}_{i+1}}$.
(4) Generate the finite element discrete system under $\widetilde{\mathscr{T}_{i+1}}$ (whose corresponding variational problem is given in (2.12)).

$$\widetilde{A}_{i+1}\widetilde{U}_{i+1} = \widetilde{F}_{i+1}, \tag{2.13}$$

and solve the resulting system to obtain the finite element solution $\widetilde{u}_{i+1}$.

where

(a): The error indicator of the element

$$\eta^2_{\widetilde{\mathscr{T}}}(\widetilde{u}, \tau) = h_\tau^2 \|R(\widetilde{u})\|^2_{0,\tau} + \sum_{e \in \partial\tau \setminus \partial\Omega} h_\tau \|J(\widetilde{u})\|^2_{0,e},$$

where

$$\begin{aligned} R(\widetilde{u})|_\tau &= f|_\tau - \mathbf{L}\widetilde{u}|_\tau, \ J(\widetilde{u})|_e = [\mathscr{L}^T(n_x, n_y, n_z) D \mathscr{L}(\partial_x, \partial_y, \partial_z)\widetilde{u}|_\tau]|_e, \\ [q]|_e &= (q|_{\tau_1})|_e - (q|_{\tau_2})|_e. \end{aligned}$$

(b): For a given Dörfler parameter $\theta \in (0,1)$, $\mathscr{M}_{\widetilde{\mathscr{T}}}$ is the subset satisfying

$$\eta^2_{\widetilde{\mathscr{T}}}(\widetilde{u}, \mathscr{M}_{\widetilde{\mathscr{T}}}) \geq \theta \eta^2(\widetilde{u}, \widetilde{\mathscr{T}}),$$

with the minimal number of elements, where

$$\eta^2_{\widetilde{\mathscr{T}}}(\widetilde{u}, \mathscr{M}_{\widetilde{\mathscr{T}}}) = \sum_{\tau \in \mathscr{M}_{\widetilde{\mathscr{T}}}} \eta^2_{\widetilde{\mathscr{T}}}(\widetilde{u}, \tau), \ \eta^2(\widetilde{u}, \widetilde{\mathscr{T}}) = \sum_{\tau \in \widetilde{\mathscr{T}}} \eta^2_{\widetilde{\mathscr{T}}}(\widetilde{u}, \tau).$$

In [9], the authors developed a LMG method for linear finite element discretizations of two-dimensional elasticity problems. Based on this, we extend the idea in [9] to three-dimensional elasticity problems and design a local multigrid method based on higher-order finite element equations. Numerical experiments demonstrate the effectiveness of this LMG method (see [20]). This paper will provide the corresponding convergence analysis of the LMG method for the corresponding higher-order finite element discretization (2.13).

3. The LMG Method for Solving Adaptive Finite Element Equations

3.1. **The LMG method for solving adaptive finite element equations.** The LMG algorithm for solving the general finite element system (2.13) of three-dimensional elasticity problems on the mesh $\widetilde{\mathscr{T}}_{i+1}$ is presented below.

For this purpose, let $\mathbb{V}(\mathscr{P}_1,\mathscr{T}_k)$ $(k=0(1)i+1)$ denote the linear finite element space on the mesh $\widetilde{\mathscr{T}}_k$, with the corresponding finite element stiffness matrix denoted by $\widetilde{A}_k^l$. Let $P_{i+1}^{p,1}$ be the restriction matrix from $\mathbb{V}(\mathscr{P}_p,\mathscr{T}_{i+1})$ to $\mathbb{V}(\mathscr{P}_1,\mathscr{T}_{i+1})$, and let P_k^{k-1} ($k=1,\cdots,i+1$) denote the restriction matrix from $\mathbb{V}(\mathscr{P}_1,\mathscr{T}_k)$ to $\mathbb{V}(\mathscr{P}_1,\mathscr{T}_{k-1})$.

Here we present the description of the LMG algorithm for solving (2.13).

Algorithm 3.1. *(LMG-Vcycle) Given the m-th iterative solution vector $\widetilde{U}^{(m)}$ obtained by the LMG method for solving (2.13), the procedure for computing the $(m+1)$ -th iterative solution vector $\widetilde{U}^{(m+1)}$ consists of the following steps.*

Step1: *Apply pre-smoothing to the residual equation $\widetilde{A}_{i+1}X=\widetilde{F}_{i+1}-\widetilde{A}_{i+1}\widetilde{U}^{(m)}$. Using zero as the initial vector, perform one-point Gauss-Seidel smoothing to obtain the solution vector e;*

Step 2: *Let $\widetilde{U}^{m,f}=\widetilde{U}^{(m)}+e$, and compute the restriction of the residual onto $\mathbb{V}(\mathscr{P}_1,\mathscr{T}_{i+1})$*

$$\widetilde{r}_{i+1}^l=P_{i+1}^{p,1}(\widetilde{F}_{i+1}-\widetilde{A}_{i+1}\widetilde{U}^{m,f})$$

Step 3: *For $k=i+1(-1)1$*

(3.1) Apply pre-smoothing to the residual equation $\widetilde{A}_k^lX=\widetilde{r}_k^l$. With zero as the initial vector, perform a single local-point Gauss-Seidel smoothing operation to obtain the solution vector e_k;

(3.2) Compute the restriction of the residual onto the space $\mathbb{V}(\mathscr{P}_1,\mathscr{T}_{k-1})$

$$\widetilde{r}_{k-1}^l=P_k^{k-1}(\widetilde{r}_k^l-\widetilde{A}_k^le_k).$$

Step 4: *Solve the residual equation on the space $\mathbb{V}(\mathscr{P}_1,\mathscr{T}_0)$, $\widetilde{A}_0X=\widetilde{r}_0^l$. The resulting solution vector is denoted as e_0;*

Step 5: *For $k=1(1)i+1$*

(5.1) Coarse grid correction: $e_k:=e_k+(P_k^{k-1})^Te_{k-1}$;

(5.2) Compute the new residual: $\widetilde{r}_k^l:=\widetilde{r}_k^l-\widetilde{A}_k^le_k$;

(5.3) Perform post-smoothing: using the zero vector as the initial guess, perform one iteration of local-point Gauss-Seidel smoothing on the residual equation as $\widetilde{A}_k^lX=\widetilde{r}_k^l$ we obtain the resulting solution vector e;

(5.4) Smoothing correction: $e_k:=e_k+e$.

Step 6: *Coarse grid correction*

(6.1) Coarse grid correction: $\widetilde{U}^{m,f}:=\widetilde{U}^{m,f}+(P_{i+1}^{p,1})^Te_{i+1}$;

(6.2) Compute the updated residual: $\widetilde{r}_{i+1} := \widetilde{F}_{i+1} - \widetilde{A}_{i+1}\widetilde{U}^{m,f}$;

(6.3) Perform post-smoothing: Apply to the residual equation $\widetilde{A}_{i+1}X = \widetilde{r}_{i+1}$. *Using the zero vector as the initial guess, perform a single-point Gauss-Seidel smoothing iteration to obtain the solution vector e;*

(6.4) Smoothing correction: $\widetilde{U}^{m,b} := \widetilde{U}^{m,f} + e$.

Remark 3.2. *For a fixed k, the local smoothing operation described above is applied only to the matrix rows corresponding to: All newly added nodes in the transition from* $\widetilde{\mathscr{T}_{k-1}}$ *to* $\widetilde{\mathscr{T}_k}$, *and their parent nodes (specifically, the two endpoints of the edge in* $\widetilde{\mathscr{T}_{k-1}}$ *to which each new node is attached).*

We now present the convergence analysis of the LMG Algorithm 3.1.

4. Convergence Analysis of the LMG Method

4.1. **Uniformly bisection-refined meshes and their corresponding finite element subspace sequences.** This subsection introduces a uniformly bisection-refined mesh sequence $\{\overline{\mathscr{T}}_k\}_{k=0}^{\infty}$, which serves as an auxiliary mesh sequence for future applications of the BPX theory under uniformly refined meshes.

For a given initial mesh $\mathscr{T}_0$, which serves as the base level of uniformly bisection-refined meshes, we obtain the following pairing set with respect to the initial mesh by applying the longest-edge refinement principle, $\overline{\mathscr{T}}_0 := \{(\tau, e) : \tau \in \mathscr{T}_0\}$, where e denotes the refinement edge (or longest edge) of element τ. Given the uniformly bisection-refined mesh sequence $\{\overline{\mathscr{T}}_k\}_{k=0}^{i-1}$ ($i \geq 1$), one sees that $\overline{\mathscr{T}}_i := \overline{\mathscr{T}}_{i-1} + \{b_\tau : \tau \in \overline{\mathscr{T}}_{i-1}\}$, where, for any pair $(\tau, e) \in \overline{\mathscr{T}}_{i-1}$, a single bisection of element τ is as follow

$$b_\tau : \{(\tau, e)\} \to \{(\tau_1, e_1), (\tau_2, e_2)\}. \tag{4.1}$$

Here τ_l and e_l ($l = 1, 2$) are illustrated in Figure 1.

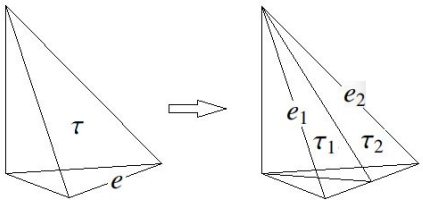

FIGURE 1. A single bisection b_τ of element τ

Remark 4.1. *The* b_τ *defined by (4.1) essentially represents a bisection refinement principle. For the 2D case, it can be proved that* e_l *serves as both the newest vertex edge and the longest edge of* τ_l. *However, this conclusion generally does not hold for 3D cases. Consequently, the corresponding longest-edge refinement algorithm becomes more complex, and requires contamination of more elements to maintain mesh conformity during refinement.*

The mesh sequence $\{\overline{\mathscr{T}}_k\}_{k=0}^{\infty}$ is required to satisfy

Condition (B1): $\overline{\mathscr{T}}_k$ is a conforming mesh.

Let $\overline{\mathbb{V}}_k$ denote the linear finite element space associated with the mesh $\overline{\mathscr{T}}_k$. Then

$$\overline{\mathbb{V}}_k := = \left\{ v \in (H_0^1(\Omega))^3 \ : \ v\big|_\tau \in (\mathscr{P}_1(\tau))^3, \forall \tau \in \overline{\mathscr{T}}_k \right\}, \tag{4.2}$$

where $\mathscr{P}_1(\tau)$ denotes the space of piecewise linear polynomials over element τ.

Since we always assume that the element sizes in the initial mesh $\mathscr{T}_0$ are of $O(1)$, the sequence $\overline{\mathscr{T}}_k$ under the longest-edge refinement principle is a quasi-uniform mesh sequence. This naturally satisfies the shape regularity condition. For any element $\tau \in \overline{\mathscr{T}}_k$, we have $h_\tau \backsimeq \bar{\gamma}^k$, where $\bar{\gamma}$ is a constant belonging to $(0,1)$, and h_τ is the length of the longest edge of the element τ.

Remark 4.2. *For a uniform bisection grid sequence $\{\overline{\mathscr{T}}_k\}_{k=0}^{\infty}$ to satisfy condition (B1), the requirement essentially applies to the initial grid $\mathscr{T}_0$. The reason is as follows: For any given initial grid $\mathscr{T}_0$, under the bisection refinement rule (the longest-edge bisection rule—if a triangle to be refined has multiple longest edges, ensure mesh conformity while minimizing the number of elements in the uniformly bisected grid), the sequence $\{\overline{\mathscr{T}}_k\}_{k=0}^{\infty}$ is uniquely determined by $\mathscr{T}_0$. It is worth noting that not all $\mathscr{T}_0$ satisfy condition (B1) under the bisection refinement rule defined in (4.1). For example, the initial grid given in Figure 2 produces a uniformly bisected grid $\overline{\mathscr{T}}_1$ that fails to meet the conformity requirement.*

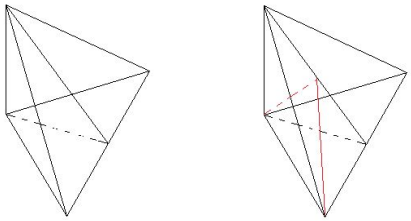

FIGURE 2. A uniformly bisected grid $\overline{\mathscr{T}}_1$ that fails to meet the conformity requirement.

4.2. **Bisection-refined grids and their finite element subspace sequences.** The sequence of bisection-refined grids is introduced for the purpose of theoretical analysis. Note that while the final level of this bisection-refined grid sequence coincides with the actual refined grid, the intermediate refinement levels generally differ from those in the practical refinement process.

Let $\mathscr{T}_0$ be the initial mesh on domain Ω, and let $\mathscr{T}_N$ be the final refined mesh level (i.e., $\widetilde{\mathscr{T}_{i+1}}$). It can be viewed as obtained through the following sequence of bisection steps, namely:

$$\begin{array}{ccccccccc} \mathscr{T}_0 & \to & \mathscr{T}_1 & \to & \mathscr{T}_2 & \cdots & \to & \mathscr{T}_N \\ & \uparrow & & \uparrow & & \cdots & \uparrow & \\ & b_1 & & b_2 & & \cdots & b_N & \end{array} \tag{4.3}$$

where $\mathscr{T}_{i-1} \to \mathscr{T}_i$ denotes

$$\mathscr{T}_i = \mathscr{T}_{i-1} + b_i, \ i = 1, \cdots, N,$$

$b_i := b_e = \{b_{\tau_1}, \cdots, b_{\tau_{\#\mathscr{R}_e}}\}$ (See [5], where edge e is required to be a compatible edge, meaning it serves as the refinement edge for all adjacent elements simultaneously, as illustrated in the left diagram of Figure 3). Here, $\mathscr{R}_e$ denotes the set of elements in $\mathscr{T}_{i-1}$ that are adjacent to edge e, that is

$$\mathscr{R}_e = \{\tau \in \mathscr{T}_{i-1} \ : \ e \subset \tau\}, \tag{4.4}$$

where $\#\mathscr{R}_e$ denotes the cardinality of $\mathscr{R}_e$, and b_τ is defined by (4.1). In particular, for an interior compatible edge e, we have $b_i := b_e = \{b_{\tau_1}, b_{\tau_2}\}$. Its mathematical behavior is illustrated in Figure 3, where x_{l_i} and x_{r_i} represent the two vertices of edge e in mesh $\mathscr{T}_{i-1}$ (also referred to as the left and right parent nodes of x_i).

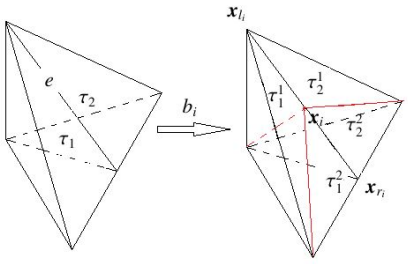

FIGURE 3. The compatible edge e and b_i in $\mathscr{T}_{i-1}$

Remark 4.3. *Two notes on (4.3):*

- **(1):** *During the algorithm implementation, the generation does not necessarily follow the order shown in (4.3). The sequence of some b_i can be swapped. Additionally, a typical encryption process usually consists of multiple encryption operations involving several b_i.*
- **(2):** *In future algorithm and theoretical analysis, nodes lying on the Dirichlet boundary in each layer of the grid $\mathscr{T}_j,\ j = 0,\cdots,N$ will not be considered.*

In the algorithm design, we require that the grid sequence $\{\mathscr{T}_i\}_{i=1}^N$ satisfies

Condition (B2): $\mathscr{T}_i$ is a shape-regular conforming mesh.

Let $\widetilde{\mathbb{V}}_i$ denote the linear finite element space associated with the mesh $\mathscr{T}_i$ as

$$\widetilde{\mathbb{V}}_i : \ = \ \left\{ v_{\mathscr{T}_i} \in (H_0^1(\Omega))^3 \ : \ v_{\mathscr{T}_i}\big|_\tau \in (\mathscr{P}_1(\tau))^3, \forall \tau \in \mathscr{T}_i \right\}, \tag{4.5}$$

where $\mathscr{P}_1(\tau)$ denotes the piecewise linear polynomials on the element τ.

Next, we introduce the concept of generation for elements and nodes in the bisection-refined grid sequence $\{\mathscr{T}_l\}$. Since the defining component b_τ is identical in both grid sequences $\overline{\mathscr{T}}_l$ and $\mathscr{T}_l$, for any given element τ in an arbitrarily bisection-refined mesh $\mathscr{T}_i$, there exists some index k such that τ coincides with an element in $\overline{\mathscr{T}}_k$. From Figure 4, We can observe that the element τ_1 in $\mathscr{T}_1$ corresponds to an element in $\overline{\mathscr{T}}_1$, and the element τ_2 in $\mathscr{T}_1$ matches an element in $\overline{\mathscr{T}}_0$.

Let $\mathscr{T}_i$ be an arbitrarily given mesh. For $\forall \tau \in \mathscr{T}_i$, if there exists some $k \geq 0$ such that $\tau \in \overline{\mathscr{T}}_k$, then we define the generation g_τ of element τ to be k. For any node $x_p \in \mathscr{T}_i$, if there exists a minimal $k \geq 0$ such that $x_p \in \overline{\mathscr{T}}_k$, then we define the generation g_p of node x_p to be k.

We specifically denote by L the maximum generation value of elements in the mesh sequence $\{\mathscr{T}_l : \ l = 0,\cdots,N\}$. It can be readily seen that any element in the bisection-refined mesh sequence $\{\mathscr{T}_l : \ l = 0,\cdots,N\}$ must coincide with some element in the uniformly bisection-refined mesh sequence $\{\overline{\mathscr{T}}_k : \ k = 0,\cdots,L\}$. Therefore, based on the definitions of the finite element spaces in (4.2) and (4.5), we conclude that $\widetilde{\mathbb{V}}_0 \subset \cdots \subset \widetilde{\mathbb{V}}_N \subseteq \overline{\mathbb{V}}_L$.

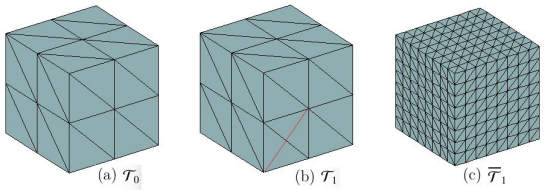

FIGURE 4. Subfigure (a) shows the initial mesh $\mathcal{T}_0$; Subigure(b) displays the mesh $\mathcal{T}_1$ obtained by performing a single b_{e_1} refinement on edge e_1 of $\mathcal{T}_0$; Subfigure (c) presents the uniformly bisected mesh $\overline{\mathcal{T}}_1$ generated from $\mathcal{T}_0$.

Let $\mathcal{N}(\mathcal{T}_i)$ and $\mathcal{E}(\mathcal{T}_i)$ denote the sets of all nodes and all edges in mesh $\mathcal{T}_i$, respectively. For any node $x_p \in \mathcal{N}(\mathcal{T}_i)$ in mesh $\mathcal{T}_i$, we define its first ring neighborhood as $\mathcal{R}_{x_p} = \{\tau \in \mathcal{T}_i \,:\, x_p \in \tau\}$. For any $e \in \mathcal{E}(\mathcal{T}_i)$, its first ring neighborhood $\mathcal{R}e$ is defined by (4.4) (with $\mathcal{T}_{i-1}$ taken as $\mathcal{T}_i$). Furthermore, we respectively define the local patches associated with node x_p and edge e (as illustrated in Figure 5).

$$\omega_p = \cup_{\tau\in\mathcal{R}_{x_p}}\tau,\ \omega_e = \cup_{\tau\in\mathcal{R}_e}\tau, \tag{4.6}$$

and the local patch $\tilde{\omega}_i$ associated with $X_i = \{x_i, x_{l_i}, x_{r_i}\} \subset \mathcal{N}(\mathcal{T}_i)$ is illustrated in Figure 6, that is

$$\tilde{\omega}_i = \omega_i \cup \omega_{l_i} \cup \omega_{r_i}. \tag{4.7}$$

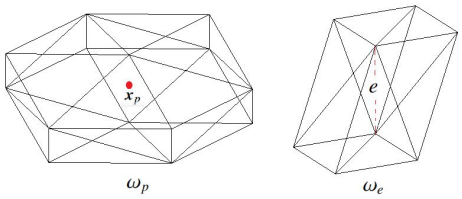

FIGURE 5. The local patches ω_p and ω_e , associated with node x_p and edge e, respectively.

We now establish the relationship between the generation of elements in $\tilde{\omega}_i$ and the generation of node x_i. From the shape regularity of the mesh, there exists a positive integer g_0 that depends only on the shape regularity of the initial mesh $\mathcal{T}_0$, such that for any given element $\tau_p \in \tilde{\omega}_i$, the following holds

$$g_i + \frac{g_0}{2} \geq g_{\tau_p} \geq g_i - \frac{g_0}{2}. \tag{4.8}$$

The following lemma presents the relationship between the generations of nodes in the set X_i.

Lemma 4.4. *The relationship between the generations of node x_i and nodes x_{l_i}, x_{r_i} (as illustrated in the right panel of Figure 3) is $g_{l_i} < g_i,\ g_{r_i} < g_i$.*

Let $\dot{\omega}_i$ denote the interior of ω_i. The following lemma establishes the relationship between the generations of any two nodes x_i, x_j in mesh $\mathcal{T}_N$ that share a certain "adjacent" relationship.

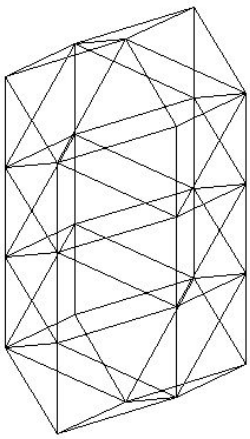

FIGURE 6. The local patch $\tilde{\omega}_i$ associated with $X_i = \{x_i, x_{l_i}, x_{r_i}\} \subset \mathcal{N}(\mathcal{T}_i)$.

Lemma 4.5 ([5]). *If node x_j is created after node x_i, and $\dot{\tilde{\omega}}_i \cap \dot{\tilde{\omega}}_j \neq \emptyset$, then the relationship between the generations of nodes x_i and x_j satisfies $g_j \geq g_i - g_0$, where g_0 is a positive integer that depends only on the shape regularity of the initial mesh $\mathcal{T}_0$.*

According to [5], we have the following lemma.

Lemma 4.6. *For the mesh sequence $\{\mathcal{T}_i\}_{i=1}^N$ in (4.3), let any two nodes x_i and x_j satisfy $i \neq j$ and $g_j = g_i > 0$. Then, $\dot{\omega}_i \cap \dot{\omega}_j = \emptyset$.*

For any element $\tau_0 \in \mathcal{T}_0$, we always assume $h_{\tau_0} = O(1)$. For any conforming mesh $\mathcal{T}$ obtained by uniform bisection refinement from $\mathcal{T}_0$, we adopt similar notation as before: $\mathcal{R}_p$ denotes the set of elements adjacent to node x_p in the mesh, ω_p represents the patch of elements surrounding x_p. If x_l is a node in $\mathcal{T}$ satisfying $g_l = \max_{x_q \in \mathcal{R}_l} g_q$, then, for any $\tau \in \omega_l$, we have $g_\tau = g_l$ and $h_\tau \backsimeq \tilde{\gamma}^{g_l}, \tilde{\gamma} \in (0,1)$, where $h_\tau = |\tau|^{\frac{1}{2}}$. For the mesh $\mathcal{T}_N$, defined in (4.3), let $\mathbb{V} := \mathbb{V}(\mathcal{P}_p, \mathcal{T}_N)$ denote the corresponding finite element space of degree p, where $n = \dim(\mathbb{V})$ represents its dimension. Then the algebraic system corresponding to the discrete variational problem (2.12) can be expressed as

$$A_N U_N = G_N, \tag{4.9}$$

where A_N is an $n \times n$ matrix, and U_N, G_N are n-dimensional vectors.

The following presents the LMG algorithm for solving the algebraic system (4.9) and its convergence analysis.

4.3. **LMG algorithm based on variable molecular problem and SSC convergence theory.** To meet the needs of the LMG algorithm description and theoretical analysis, several subspaces and corresponding variational subproblems are introduced.

4.3.1. *Subspaces and variational subproblems.* The spaces $\mathbb{V}_i$, $i = 1, \cdots, N$.

Let x_i $(1 \leq i \leq N)$ be the i-th non-Dirichlet node in the grid $\mathcal{T}_i$ after removing the nodes from the initial grid $\mathcal{T}_0$, and denote the set X_i as $X_i = \{x_i, x_{l_i}, x_{r_i}\}$, where x_{l_i} and x_{r_i} be the two endpoints of the edge in grid $\mathcal{T}_{i-1}$ that has x_i as its midpoint (as shown in the right panel of Figure 3).

The linear finite element subspace $\mathbb{V}_i$ is defined as follows:

$$\mathbb{V}_i = \text{span}\{\Psi^i_{3i-2}, \Psi^i_{3i-1}, \Psi^i_{3i}, \Psi^i_{3l_i-2}, \Psi^i_{3l_i-1}, \Psi^i_{3l_i}, \Psi^i_{3r_i-2}, \Psi^i_{3r_i-1}, \Psi^i_{3r_i}\}, \tag{4.10}$$

where

$$\Psi^i_{3p-2} = \begin{pmatrix} \psi^i_p \\ 0 \\ 0 \end{pmatrix}, \ \Psi^i_{3p-1} = \begin{pmatrix} 0 \\ \psi^i_p \\ 0 \end{pmatrix}, \ \Psi^i_{3p} = \begin{pmatrix} 0 \\ 0 \\ \psi^i_p \end{pmatrix},$$

where the function ψ^i_p is the linear basis function at node x_p ($x_p \in X_i$) on the grid $\mathscr{T}_i$. Obviously, $\Psi^i_{3p-2}, \Psi^i_{3p-1}, \Psi^i_{3p} \in \widetilde{\mathbb{V}}_i$. Clearly, $\mathbb{V}_i$ is the space of piecewise linear polynomials on the grid $\mathscr{T}_i$, and thus we have $\mathbb{V}_i \subseteq \mathbb{V}$.

Remark 4.7. *When defining $\mathbb{V}_i$, if the node x_{l_i} or the node x_{r_i} is a Dirichlet node, without loss of generality, let x_{l_i} be the Dirichlet node, then (4.10) becomes*

$$\mathbb{V}_i = \text{span}\{\Psi^i_{3i-2}, \Psi^i_{3i-1}, \Psi^i_{3i}, \Psi^i_{3r_i-2}, \Psi^i_{3r_i-1}, \Psi^i_{3r_i}\},$$

If the node x_i is a non-Dirichlet node, but both x_{l_i} and x_{r_i} are Dirichlet nodes, then (4.10) may also be $\mathbb{V}_i = \text{span}\{\Psi^i_{3i-2}, \Psi^i_{3i-1}, \Psi^i_{3i}\}$.

Additionally, denote the linear finite element subspace associated with the initial mesh $\mathscr{T}_0$ as $\mathbb{V}_0 = \mathbb{V}(\mathscr{P}_1, \mathscr{T}_0)$. $\mathbb{V}_{N+k}$, $k = 1, \cdots, n_2$. For any $k (k = 1, \cdots, n_2)$, we define the finite element subspace on the mesh $\mathscr{T}_N$ as

$$\mathbb{V}_{N+k} = \text{span}\{\Phi_{3k-2}, \Phi_{3k-1}, \Phi_{3k}\} \subset \mathbb{V},$$

and let $J := N + n_2$. Assume that the variational problem defined on the subspace $\mathbb{V}_k$ satisfies the following variational problem $a_k(u,v) = a(u,v)$ for all $u, v \in \mathbb{V}_k, k = 0(1)J$.

We provide the algorithmic of the LMG method for solving problem (4.9) as follow.

4.3.2. *The algorithmic of the LMG method.* Given the l-th iterative solution $u_l \in \mathbb{V}$ for the discrete problem (4.9), the $(l+1)$-th iterative solution $u_{l+1} \in \mathbb{V}$ can be obtained through the following algorithm:

Algorithm 4.8 (LMG method)**.**

Step1: *(Pre-smoothing) Solve exactly each 2-th order variational subproblem (ordered canonically).*

$$\begin{aligned}
&u^0_{l,1} = u_l;\\
&\text{do } i = 1(1)n_2\\
&\ \textit{Find } e_i \in \mathbb{V}_{N+i} \textit{ such that it satisfies}\\
&\ a(e_i, w_i) = F(w_i) - a(u^{i-1}_{l,1}, w_i), \ \forall w_i \in \mathbb{V}_{N+i};\\
&\ u^i_{l,1} = u^{i-1}_{l,1} + e_i;\\
&\text{enddo}\\
&u_{l,1} := u^n_{l,1}.
\end{aligned} \tag{4.11}$$

Step2: *(Pre-smoothing) Solve exactly the variational subproblems for the linear element subspaces* $\mathbb{V}_i$, $i = 1(1)N$.

$$\begin{aligned}
&u_{l,2}^0 = u_{l,1};\\
&\text{do } i = 1(1)N\\
&\ \textit{Find } e_i \in \mathbb{V}_i \textit{ such that it satisfies}\\
&\ a(e_i, w_i) = F(w_i) - a(u_{l,2}^{i-1}, w_i),\ \forall w_i \in \mathbb{V}_i;\\
&\ u_{l,2}^i = u_{l,2}^{i-1} + e_i;\\
&\text{enddo}\\
&u_{l,2} = u_{l,2}^N.
\end{aligned} \tag{4.12}$$

Step3: *(Coarse grid correction) Compute exact solutions to the variational subproblems on the linear finite element subspace* $\mathbb{V}_0$.

Find $e_0 \in \mathbb{V}_0$ *such that it satisfies*

$$\begin{aligned}
&a(e_0, w_1) = F(w_1) - a(u_{l,2}, w_1), \forall\ w_1 \in \mathbb{V}_0;\\
&u_{l,3} = u_{l,2} + e_0.
\end{aligned}$$

Step4: *(Post-smoothing) Solve exactly the variational subproblems for the linear element subspaces* $\mathbb{V}_i, i = N(-1)1$.

$$\begin{aligned}
&u_{l,4}^{N+1} = u_{l,3};\\
&\text{do } i = N(-1)1\\
&\ \textit{Find } \ e_i \in \mathbb{V}_i, \textit{ such that it satisfies}\\
&\ a(e_i, w_i) = F(w_i) - a(u_{l,4}^{i+1}, w_i),\ \forall w_i \in \mathbb{V}_i;\\
&\ u_{l,4}^i = u_{l,4}^{i+1} + e_i;\\
&\text{enddo}\\
&u_{l,4} = u_{l,4}^1.
\end{aligned} \tag{4.13}$$

Step5: *(Post-smoothing) Solve exactly each* 2*-th order variational subproblem (ordered canonically).*

$$\begin{aligned}
&u_{l,5}^{n_2+1} = u_{l,4};\\
&\text{do } i = n_2(-1)1\\
&\ \textit{Find } e_i \in \mathbb{V}_{N+i}, \textit{ such that it satisfies}\\
&\ a(e_i, w_i) = F(w_i) - a(u_{l,5}^{i+1}, w_i),\ w_1 \in \mathbb{V}_{N+i};\\
&\ u_{l,5}^i = u_{l,5}^{i+1} + e_i;\\
&\text{enddo}\\
&u_{l+1} = u_{l,5}^1.
\end{aligned} \tag{4.14}$$

Remark 4.9. *A comparison between Algorithm 3.1 and Algorithm 4.8 reveals that during smoothing operations (which constitute the core of the LMG algorithm), the subsystems of linear algebraic equations involved at each grid level and the rows requiring smoothing remain*

identical - the only difference lies in their smoothing sequence. Consequently, for theoretical analysis purposes, Algorithm 4.8 can be employed as a substitute for Algorithm 3.1.

4.3.3. *Convergence Theory of SSC for LMG Algorithm.* We now analyze a simplified version of the LMG Algorithm 4.8, where only the coarse-grid correction (in which case $u_{l,2} = u_l$) and post-smoothing are performed, and derive its convergence rate estimate.

By applying the theory of successive subspace correction (SSC) [19], we obtain that the convergence rate of the simplified LMG Algorithm 4.8 is given by $\rho = 1 - \frac{1}{1+c_0}$, where

$$c_0 = \sup_{\|v\|_A=1} \inf_{\sum_{k=0}^{J} v_k = v} \sum_{k=0}^{J} \|P_k \sum_{j=k+1}^{J} v_j\|_A^2,$$

where $P_k : \mathbb{V} \to \mathbb{V}_k$ is the energy projection operator.

To estimate c_0, we need to introduce the following conditions (P1) and (P2).

(P1): (**Stable decomposition**): For any $v \in \mathbb{V}$, there exists a decomposition $v = \sum_{k=0}^{J} v_k, v_k \in \mathbb{V}_k, k = 0, \cdots, J$, such that

$$\sum_{k=0}^{J} \|v_k\|_A^2 \leq K_0 \|v\|_A^2, \tag{4.15}$$

where K_0 is a positive constant.

(P2): (**Strong Cauchy-Schwarz Inequality**): For any $u_k, v_k \in \mathbb{V}_k, k = 0, \cdots, J$, such that

$$\Big| \sum_{k=0}^{J} \sum_{j=k+1}^{J} (u_k, v_j)_A \Big| \leq K_1 \Big(\sum_{k=0}^{J} \|u_k\|_A^2 \Big)^{1/2} \Big(\sum_{k=0}^{J} \|v_k\|_A \Big)^{1/2}, \tag{4.16}$$

where K_1 is a positive constant.

By utilizing conditions (P1) and (P2), we can derive the following upper bound estimate for ([19])

$$c_0 \leq K_0 K_1^2. \tag{4.17}$$

We now examine whether conditions (P1) and (P2) hold for the LMG Algorithm 4.8. To this end, we first introduce the Scott-Zhang quasi-interpolation operator and present its relevant properties.

4.4. Scott-Zhang quasi-interpolation operator. 1. Scott-Zhang Quasi-Interpolation Operator on a Single Mesh Level $\mathscr{T}$ and Its Properties

By utilizing the definition of the scalar-valued Scott-Zhang quasi-interpolation operator $\mathscr{I}_{\mathscr{T}} : H^1(\Omega) \mapsto \mathscr{V}(\mathscr{P}_1, \mathscr{T})$, from [5, 13], we can define the Scott-Zhang interpolation operator for three-dimensional vector spaces.

$$\mathscr{Q}_{\mathscr{T}} = (\mathscr{I}_{\mathscr{T}}, \mathscr{I}_{\mathscr{T}}, \mathscr{I}_{\mathscr{T}})^T, \tag{4.18}$$

and for any $v \in (H^1(\Omega))^3$, the operator satisfies that $\mathscr{Q}_{\mathscr{T}} v = (\mathscr{I}_{\mathscr{T}} v_1, \mathscr{I}_{\mathscr{T}} v_2, \mathscr{I}_{\mathscr{T}} v_3)^T$, where

$$\begin{aligned}
\mathscr{I}_{\mathscr{T}} v_1 &= \sum_{x_p \in \mathscr{N}(\mathscr{T})} \left((\int_{\tau_p} \theta_p v_1 dx) \Psi_{3p-2} \right), \\
\mathscr{I}_{\mathscr{T}} v_2 &= \sum_{x_p \in \mathscr{N}(\mathscr{T})} \left((\int_{\tau_p} \theta_p v_2 dx) \Psi_{3p-1} \right), \\
\mathscr{I}_{\mathscr{T}} v_3 &= \sum_{x_p \in \mathscr{N}(\mathscr{T})} \left((\int_{\tau_p} \theta_p v_3 dx) \Psi_{3p} \right),
\end{aligned}$$

$\Psi_{3p-2} = (\psi_p, 0, 0)^T$, $\Psi_{3p-1} = (0, \psi_p, 0)^T$, $\Psi_{3p} = (0, 0, \psi_p)^T$.

We now present several key properties satisfied by the aforementioned Scott-Zhang quasi-interpolation operator $\mathscr{Q}_{\mathscr{T}}$ defined on the mesh $\mathscr{T}$.

Property 4.1. *Let x_l be an arbitrary given node in the mesh $\mathscr{T}$, and let τ_l be the supporting element associated with the node x_l . Then, at the node x_l, for all $u \in (\mathscr{P}_1(\tau_l))^3$, $(\mathscr{Q}_{\mathscr{T}} u)(x_l) = u(x_l)$.*

Let $\mathscr{N}(\mathscr{T})$ denote the set of nodes of the mesh $\mathscr{T}$. It follows that, for any given linear finite element function $u \in \mathbb{V}(\mathscr{P}_1, \mathscr{T})$, $(\mathscr{Q}_{\mathscr{T}} u)(x_p) = u(x_p)$, $\forall\, x_p \in \mathscr{N}(\mathscr{T})$.

Property 4.2. *For any $u \in \mathbb{V}(\mathscr{P}_1, \mathscr{T})$, it holds $\mathscr{Q}_{\mathscr{T}} u = u$.*

It can be proved that the quasi-interpolation operator $\mathscr{Q}_{\mathscr{T}}$ defined on the two-dimensional vector space satisfies the following approximation and stability properties.

Lemma 4.10. *Let $\mathscr{T}$ be a shape-regular mesh partition and $v \in (H^1(\Omega))^3$. Then, for any $\forall \tau \in \mathscr{T}$ and $x_p \in \mathscr{N}(\mathscr{T})$, the operator $\mathscr{Q}_{\mathscr{T}}$satisfies the following properties:*

$$\begin{aligned}
\|\mathscr{Q}_{\mathscr{T}} v\|_1 + \|h^{-1}(v - \mathscr{Q}_{\mathscr{T}} v)\| &\lesssim \|v\|_1, && (4.19)\\
\|(v - \mathscr{Q}_{\mathscr{T}} v)\|_{0,\tau} &\lesssim h_\tau |v|_{1,\Omega_\tau}, && (4.20)\\
\|\mathscr{Q}_{\mathscr{T}} v\|_{0,\tau} &\lesssim \|v\|_{0,\Omega_\tau} && (4.21)\\
h_{\tau_p}^2 |\mathscr{Q}_{\mathscr{T}} v(x_p)|^2 &\lesssim \|v\|_{\tau_p}^2, && (4.22)
\end{aligned}$$

where $|\mathscr{Q}_{\mathscr{T}} v(x_p)|^2 = |\mathscr{I}_{\mathscr{T}} v_1(x_p)|^2 + |\mathscr{I}_{\mathscr{T}} v_2(x_p)|^2 + |\mathscr{I}_{\mathscr{T}} v_3(x_p)|^2$, $h := h(x) = h_\tau$, $x \in \tau$, $\Omega_\tau = \cup_{e \in \partial\tau} \omega_e$, τ_p represents any chosen element from those adjacent to the node x_p, h_{τ_p} characterizing the mesh size of element τ_p .

2. Scott-Zhang Quasi-Interpolation Operator and Its Properties on Bisection-Generated Mesh Sequence $\{\mathscr{T}_i\}_{i=0}^N$

• Definition of the Scott-Zhang Interpolation Operator

We first define the Scott-Zhang quasi-interpolation operator on the bisection-refined mesh $\mathscr{T}_N$ as specified in (4.3). Note that $\mathbb{V} \subset (H^1(\Omega))^3$. Then, using the definition of the Scott-Zhang interpolation operator on a single mesh level (4.18), we can define the Scott-Zhang interpolation operator from $\mathbb{V}$ to $\widetilde{\mathbb{V}}_N$, $\mathscr{Q}_{\mathscr{T}_N} = (\mathscr{I}_N, \mathscr{I}_N, \mathscr{I}_N)^T$, where $\mathscr{T}$ denotes $\mathscr{T}_N$ in equation (4.18),

Next, we define the sequence of Scott-Zhang quasi-interpolation operators $\{\mathscr{Q}_i\}_{i=0}^N$ on the sequence of bisection-refined meshes $\{\mathscr{T}_i\}_{i=0}^N$ (defined by (4.3)), recursively.

(1) The definition of the Scott-Zhang quasi-interpolation operator $\mathscr{Q}_0$ on the initial mesh $\mathscr{T}_0$.

Let $\mathbb{V}(\mathscr{P}_1,\mathscr{T}_0)$ denote the linear finite element space on the mesh $\mathscr{T}_0$. Using the definition of the Scott-Zhang interpolation operator on a single mesh (see (4.18)), we define the Scott-Zhang interpolation operator $\mathscr{Q}_0:\overline{\mathbb{V}}_L\mapsto\widetilde{\mathbb{V}}_0$ such that, for any given $u=(u_1,u_2,u_3)^T\in\mathbb{V}(\mathscr{P}_1,\mathscr{T}_N)$, we have

$$\mathscr{Q}_0u = \sum_{x_p\in\mathscr{N}(\mathscr{T}_0)}(c_p^{1,0}\Psi_{3p-2}^0+c_p^{2,0}\Psi_{3p-1}^0+c_p^{3,0}\Psi_{3p}^0), \tag{4.23}$$

where the basis functions $\Psi_{3p-2}^0=(\psi_p^0,0,0)^T$, $\Psi_{3p-1}^0=(0,\psi_p^0,0)^T$, $\Psi_{3p}^0=(0,0,\psi_p^0)^T$, ψ_p^0denotes the linear basis function at node x_p in mesh $\mathscr{T}_0$, and $c_p^{l,0}=\int_{\tau_p}\theta_pu_ldx, l=1,3$, for with τ_p being an arbitrary element adjacent to node x_p.

(2) Suppose that the Scott-Zhang quasi-interpolation operator $\mathscr{Q}_{i-1}:\overline{\mathbb{V}}_L\to\widetilde{\mathbb{V}}_{i-1}$ has been defined, with its expression given by

$$\begin{aligned}\mathscr{Q}_{i-1}u &= \sum_{x_p\in\mathscr{N}(\mathscr{T}_{i-1}),x_p\notin X_i}(c_p^{1,i-1}\Psi_{3p-2}^{i-1}+c_p^{2,i-1}\Psi_{3p-1}^{i-1}+c_p^{3,i-1}\Psi_{3p}^{i-1})\\ &+ \sum_{x_p\in X_i\setminus x_i}(c_p^{1,i-1}\Psi_{3p-2}^{i-1}+c_p^{2,i-1}\Psi_{3p-1}^{i-1}+c_p^{3,i-1}\Psi_{3p}^{i-1}).\end{aligned} \tag{4.24}$$

We now define the Scott-Zhang quasi-interpolation operator $\mathscr{Q}_i$ on mesh $\mathscr{T}_i$. Let $\widetilde{\mathbb{V}}_i$ be the linear finite element space associated with mesh $\mathscr{T}_i$ as defined in (4.5). Then the operator $\mathscr{Q}_i:\overline{\mathbb{V}}_L\mapsto\widetilde{\mathbb{V}}_i$ is given by

$$\begin{aligned}\mathscr{Q}_iu &= \sum_{x_p\in\mathscr{N}(\mathscr{T}_{i-1}),x_p\notin X_i}(c_p^{1,i-1}\Psi_{3p-2}^{i-1}+c_p^{2,i-1}\Psi_{3p-1}^{i-1}+c_p^{3,i-1}\Psi_{3p}^{i-1})\\ &+ \sum_{x_p\in X_i\setminus x_i}(c_p^{1,i}\Psi_{3p-2}^{i}+c_p^{2,i}\Psi_{3p-1}^{i}+c_p^{3,i}\Psi_{3p}^{i})\\ &+ c_i^{1,i}\Psi_{3i-2}^i+c_i^{2,i}\Psi_{3i-1}^i+c_i^{3,i}\Psi_{3i}^i,\end{aligned} \tag{4.25}$$

where $\Psi_{3p-2}^i=(\psi_p^i,0,0)^T$, $\Psi_{3p-1}^i=(0,\psi_p^i,0)^T$, $\Psi_{3p}^i=(0,0,\psi_p^i)^T$, ψ_p^i is the linear basis function associated with node x_p in mesh $\mathscr{T}_i$. $c_p^{l,i}=\int_{\tau_p}\theta_pu_ldx$, $l=1,3$, where the coefficients $c_p^{1,i},c_p^{2,i},c_p^{3,i}(x_p\in X_i)$ are uniquely determined by their associated supporting element τ_p. The selection rule for the supporting element is as follows: For any node $x_p\in X_i$, we select from mesh $\mathscr{T}_i$ the element adjacent to x_p that has the largest generation value as its supporting element.

At this point, we have completed the constructive (recursive) definition of the Scott-Zhang quasi-interpolation operator $\mathscr{Q}_i:\overline{\mathbb{V}}_L\mapsto\widetilde{\mathbb{V}}_i, i=0(1)N$

• The generation values of the supporting elements for nodes adjacent to x_i in the expressions of operators $\mathscr{Q}_i$ and $\mathscr{Q}_{i-1}$.

Property 4.3. *For any i, where $i=1(1)N$, let g_i denote the generation of node x_i. Then in the definition of operator $\mathscr{Q}_i$ (see (4.25)), the following holds for the supporting elements in mesh $\mathscr{T}_i$:*

1. The generation of the supporting element for node x_i equals g_i.

2. The generations of the supporting elements for nodes x_{l_i} and x_{r_i} are greater than or equal to g_i.

Property 4.4. *For any arbitrary i, where $i = 1(1)N$, let the "generation" of node x_i be g_i. Then, when defining the operator Q_{i-1} (see (4.24)), the "generation" of the supporting cell of node x_j ($x_j \in X_i \setminus x_i$) on the grid $\mathscr{T}_{i-1}$ is greater than or equal to $g_i - 1$.*

Property 4.5. *For any i,, $i = 1(1)N$, the "generation" of the nodes x_{u_i}, x_{c_i} and x_{d_i}(as shown in Figure 7 (a)) opposite to the edge e_i where node x_i lies is equal to $g_i - 1$. Moreover, when defining the interpolation operator $\mathscr{Q}_{i-1}$ (see (4.24)), the "generation" of the supporting cells of these two nodes on the grid $\mathscr{T}_{i-1}$ is greater than or equal to $g_i - 1$.*

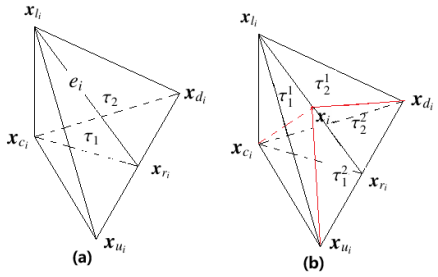

FIGURE 7. The two elements in $\mathscr{T}_{i-1}$ connected by edge e_i (Left picture) A local view of the mesh $\mathscr{T}_i$ generated after performing one bisection b_i on the mesh $\mathscr{T}_{i-1}$(Right picture).

• Two properties of the Scott-Zhang interpolation operator sequence $\{\mathscr{Q}_i\}_{i=0}^N$.

Lemma 4.11. *For any $u \in \overline{\mathbb{V}}_L$ and $x_p \in \mathscr{N}(\mathscr{T}_i)$, if $x_p \notin X_i$, then $(\mathscr{Q}_i - \mathscr{Q}_{i-1})u(x_p) = 0$.*

Lemma 4.12. *Let the generation of node x_i be g_i. For any $\bar{v}_k \in \overline{\mathbb{V}}_k \subset \overline{\mathbb{V}}_L$ ($0 \le k \le g_i - 1$), it holds that $(\mathscr{Q}_i - \mathscr{Q}_{i-1})\bar{v}_k = 0$.*

With the above preparations, we now proceed to prove that conditions (P1) and (P2) hold. The proof follows a parallel approach to that in [5].

4.5. **Proof of Condition (P1).** By utilizing the compact support property of the functions v_j ($j = 1(1)J$), we can prove that (4.15) is equivalent to the following inequality

$$\sum_{j=0}^{N} \|v_j\|^2_{A,\tilde{\omega}_j} + \sum_{k=N+1}^{J} \|v_k\|^2_{A,\tilde{\omega}_k} \lesssim K_0 \|v\|^2_A, \tag{4.26}$$

where $\tilde{\omega}_0 = \Omega$.

We now present the proof of (4.26). First, by employing Lemmas 4.6, and (4.8), we can prove the following two inequalities hold

$$\sum_{g_i=k} \|u\|^2_{\omega_i} = \|u\|^2_{\Omega_{i,k}} \le \|u\|^2_{\Omega}, \tag{4.27}$$

$$\sum_{g_i=k} \|u\|^2_{\tilde{\omega}_i} \lesssim \|u\|^2_{\Omega}, \tag{4.28}$$

where $\Omega_{i,k} = \bigcup_{g_i=k} \omega_i$.

Next, we present a space decomposition of $\mathbb{V}$. For any function $v \in \mathbb{V}$, let

$$u = \mathscr{Q}_{\mathscr{T}_N} v \in \widetilde{\mathbb{V}}_N. \tag{4.29}$$

Clearly, $u = \mathscr{Q}_N u$. We decompose $\mathscr{Q}_N u$ as follows:

$$\mathscr{Q}_N u = \sum_{i=0}^{N} v_i, \tag{4.30}$$

where

$$v_i = (\mathscr{Q}_i - \mathscr{Q}_{i-1})u \in \mathbb{V}_i,\ i = 0, \cdots, N, \tag{4.31}$$

with $\mathscr{Q}_{-1} := 0$. Observing that $v - \mathscr{Q}_N u \in \mathbb{V}$, we decompose it as follows

$$v - \mathscr{Q}_N u = \sum_{k=N+1}^{J} v_k, \tag{4.32}$$

where

$$v_k = c_k^1 \Phi_{3k-2} + c_k^2 \Phi_{3k-1} + c_k^3 \Phi_{3k} \in \mathbb{V}_k,\ k = N+1, \cdots, J, \tag{4.33}$$

and

(1): When the node x_k is a grid partition node, c_k^1, c_k^2, and c_k^3 represent the three components of the vector function $v - \mathscr{Q}_N u$ at this node, that is,

$$(c_k^1, c_k^2, c_k^3)^T = (v - \mathscr{Q}_N u)(x_k). \tag{4.34}$$

(2): When the node x_k is the midpoint of edge e_k in the mesh, the coefficients c_k^1, c_k^2, and c_k^3 can be expressed in terms of the components of the vector function $v - \mathscr{Q}_N u$ evaluated at both the endpoints and midpoint of the edge, namely,

$$(c_k^1, c_k^2, c_k^3)^T = (v - \mathscr{Q}_N u)(x_k) - \frac{1}{2}((v - \mathscr{Q}_N u)(x_k^l) + (v - \mathscr{Q}_N u)(x_k^r)), \tag{4.35}$$

where x_k^l and x_k^r are the left and right endpoints of edge e_k, respectively.

From (4.34) and (4.35), we see that

$$(c_k^1 + c_k^2 + c_k^3)^2 \lesssim \sum_{x_l \in \tilde{\mathscr{N}_k}} \left((v - \mathscr{Q}_N u)(x_l)\right)^2,$$

where $\tilde{\mathscr{N}_k}$ denotes the set of all interpolation nodes within the support of the basis function ψ_k corresponding to x_k. From equations (4.30) and (4.32), we conclude that, for any $v \in \mathbb{V}$, there exists the decomposition $v = \sum_{i=0}^{N} v_i + \sum_{k=N+1}^{J} v_k$. For the above decomposition, the following inequality can be established

$$\sum_{k=N+1}^{J} \|v_k\|_{A,\bar{\omega}_k}^2 \lesssim \frac{\lambda + \mu}{\mu} \|v\|_A^2. \tag{4.36}$$

and

$$\sum_{i=0}^{N} \|v_i\|_{A,\tilde{\omega}_i}^2 \lesssim \frac{\lambda + \mu}{\mu} \|v\|_A^2. \tag{4.37}$$

By substituting (4.36) and (4.37) into the left-hand side of (4.26) and applying (2.3), we prove that (4.26) holds. Moreover,

$$K_0 = \frac{\lambda+\mu}{\mu} = \frac{1}{1-2\nu}. \tag{4.38}$$

We first prove that (4.36) holds.

Proof. From the boundedness condition (2.7) satisfied by the bilinear form $a(\cdot,\cdot)$, we see that

$$\sum_{k=N+1}^{J} \|v_k\|_{A,\bar{\omega}_k}^2 \lesssim (\lambda+\mu) \sum_{k=N+1}^{J} \|v_k\|_{1,\bar{\omega}_k}^2, \tag{4.39}$$

Comparing (4.36) with (4.39), we see that, to prove (4.36) holds, it suffices to establish the following inequality

$$\sum_{k=N+1}^{J} \|v_k\|_{1,\bar{\omega}_k}^2 \lesssim \frac{1}{\mu}\|v\|_A^2. \tag{4.40}$$

We now prove that (4.40) holds. In fact, by employing inverse estimates and (4.33), and noting that the local discrete norm can be bounded by the continuous norm, we obtain

$$\sum_{k=N+1}^{J} \|v_k\|_{1,\bar{\omega}_k}^2 \lesssim \sum_{k=N+1}^{J} h_k^{-2}\|v_k\|_{\bar{\omega}_k}^2 \lesssim \sum_{k=N+1}^{J} h_k^{-2}\|(v-\mathscr{Q}_N u)\|_{\bar{\omega}_k}^2.$$

Consequently, by additionally utilizing $u = \mathscr{Q}_{\mathscr{T}_N} v$, (4.20), and (2.8), we can further obtain

$$\sum_{k=N+1}^{J} \|v_k\|_{1,\bar{\omega}_k}^2 \lesssim \sum_{k=N+1}^{J} \sum_{\tau\in\bar{\omega}_k} \|v\|_{1,\Omega_\tau}^2 \lesssim \sum_{\tau\in\mathscr{T}_N} \|v\|_{1,\tau}^2 \lesssim \frac{1}{\mu}\|v\|_A^2.$$

□

Next, we prove that (4.37) holds. To this end, we introduce the following three lemmas.

Let $\bar{Q}_k$ denote the L^2-projection from the space $\overline{\mathbb{V}}_L$ to $\overline{\mathbb{V}}_k$ ($k = 1,\cdots,L$) (here we set $\bar{Q}_{-1} = 0$). Following the proof of analogous properties in [1], we can establish the following properties.

Lemma 4.13. *For any $\bar{v} \in \overline{\mathbb{V}}_L$, let $\bar{v}_k = (\bar{Q}_k - \bar{Q}_{k-1})\bar{v}$ for $k = 0,\cdots,L$. Then the decomposition $\bar{v} = \sum_{k=0}^{L} \bar{v}_k$ satisfies $\sum_{k=0}^{L} \bar{h}_k^{-2}\|\bar{v}_k\|_{0,\Omega}^2 \lesssim \|\bar{v}\|_{1,\Omega}^2$.*

By utilizing the definition of the projection operator $\bar{Q}_k$ and the space nesting property $\overline{\mathbb{V}}_l \subseteq \overline{\mathbb{V}}_k$ ($l \le k$), we can prove the following orthogonality result.

Lemma 4.14 (Orthogonality)**.** *For any $u \in \overline{\mathbb{V}}_L$, let $\bar{v}_k = (\bar{Q}_k - \bar{Q}_{k-1})u$ for $k = 0,\cdots,L$. Then $(\bar{v}_i, \bar{v}_j) = \delta_{i,j}\|\bar{v}_i\|_{0,\Omega}^2$, $i,j = 0,\cdots,L$.*

Lemma 4.15 (Hardy inequality, [7])**.** *Let $\{a_k\}_{k=0}^{L}$ and $\{b_k\}_{k=0}^{L}$ be two positive sequences satisfying $b_k \le \sum_{l=k}^{L} a_l, \forall k \ge 0$. Then, for any $s \in (0,1)$, $\sum_{k=0}^{L} s^{-k} b_k \lesssim \sum_{k=0}^{L} s^{-k} a_k$.*

We now present the proof of (4.37).

Proof. From (4.29), we have $u = \mathscr{Q}_{\mathscr{T}_N} v \in \widetilde{\mathbb{V}}_N \subseteq \overline{\mathbb{V}}_L,$. Then u admits the following decomposition:

$$u = \sum_{k=0}^{L} \bar{u}_k, \tag{4.41}$$

where $\bar{u}_k = (\bar{Q}_k - \bar{Q}_{k-1})u$ for $k = 0, \cdots, L$, with $\bar{Q}_{-1} = 0$, and $\bar{Q}_k$ ($k = 1(1)L$) denotes the L^2-projection from the space $\overline{\mathbb{V}}_L$ to $\overline{\mathbb{V}}_k$. From Lemma 4.13, we conclude that the decomposition in (4.41) satisfies the following stability result

$$\sum_{k=0}^{L} \bar{h}_k^{-2} \|\bar{u}_k\|_0^2 \lesssim \|u\|_1^2. \tag{4.42}$$

For a given i ($i = 1(1)N$), when $0 \le k \le g_i - 1$, note that $\bar{u}_k \in \widetilde{\mathbb{V}}_N$. Then both $\mathscr{Q}_i \bar{u}_k$ and $\mathscr{Q}_{i-1}\bar{u}_k$ are well-defined. From Lemma 4.12, we see that $(\mathscr{Q}_i - \mathscr{Q}_{i-1})\bar{u}_k = 0$. From (4.31) and (4.41), we have $v_i = (\mathscr{Q}_i - \mathscr{Q}_{i-1}) \sum_{l=g_i}^{L} \bar{u}_l$. By employing Lemma 4.11 and noting the equivalence between local continuous norms and local discrete norms, we obtain

$$\|v_i\|_{\tilde{\omega}_i}^2 \lesssim h_i^2 \sum_{x_p \in X_i} (((\mathscr{Q}_i - \mathscr{Q}_{i-1}) \sum_{l=g_i}^{L} \bar{u}_l)(x_p))^2, \tag{4.43}$$

Let $w = \sum_{l=g_i}^{L} \bar{u}_l$. For any $x_p \in X_i$, it can be readily proved from (4.22) that

$$h_i^2((\mathscr{Q}_i w)(x_p))^2 \lesssim \|w\|_{\omega_i}^2,\ h_i^2((\mathscr{Q}_{i-1} w)(x_p))^2 \lesssim \|w\|_{\omega_i}^2. \tag{4.44}$$

Substituting (4.44) into (4.43), we obtain

$$\|v_i\|_{\tilde{\omega}_i}^2 \lesssim \| \sum_{l=g_i}^{L} \bar{u}_l \|_{\omega_i}^2. \tag{4.45}$$

Summing both sides of (4.45) over $g_i = k$ and utilizing (4.27) and Lemma 4.14, we obtain

$$\sum_{g_i=k} \|v_i\|_{\tilde{\omega}_i}^2 \lesssim \sum_{g_i=k} \| \sum_{l=g_i}^{L} \bar{u}_l \|_{\omega_i}^2 = \| \sum_{l=g_i}^{L} \bar{u}_l \|_{\Omega_{i,k}}^2 = \sum_{l=k}^{L} \|\bar{u}_l\|_{\Omega}^2.$$

Note that, under uniform refinement, the mesh size satisfies $\bar{h}_k = (\frac{1}{\sqrt{2}})^k \bar{h}_0$ (without loss of generality, take $\bar{h}_0 = O(1)$). Then

$$\sum_{k=0}^{L} \bar{h}_k^{-2} \sum_{g_i=k} \|v_i\|_{\tilde{\omega}_i}^2 \lesssim \sum_{k=0}^{L} \bar{h}_k^{-2} \|\bar{v}_k\|_{\Omega}^2.$$

Using (2.7) and (4.42) along with the inverse estimate, we obtain

$$\sum_{i=0}^{N} \|v_i\|_{A,\tilde{\omega}_i}^2 \lesssim (\lambda + \mu) \sum_{i=0}^{N} h_i^{-2} \|v_i\|_{\tilde{\omega}_i}^2 = (\lambda + \mu) \sum_{k=0}^{L} \bar{h}_k^{-2} \sum_{g_i=k} \|v_i\|_{\tilde{\omega}_i}^2 \lesssim (\lambda + \mu)\|v\|_1^2 \lesssim \frac{\lambda + \mu}{\mu} \|v\|_A^2.$$

□

Hence, we have verified that condition (P1) holds.

4.6. **Proof of condition (P2).** By the compact support property of the functions $v_j (j = 1(1)J)$, equation (4.16) is equivalent to

$$\begin{aligned} \Big|\sum_{i=0}^{J}\sum_{j=i+1}^{J}(u_i,v_j)_A\Big| \;\le\; & K_1\Big(\sum_{i=0}^{N}\|u_i\|^2_{A,\tilde{\omega}_i}+\sum_{i=N+1}^{J}\|u_i\|^2_{A,\bar{\omega}_k}\Big)^{1/2} \\ & \Big(\sum_{j=0}^{N}\|v_j\|^2_{A,\tilde{\omega}_j}+\sum_{j=N+1}^{J}\|v_j\|^2_{A,\bar{\omega}_j}\Big)^{1/2}. \end{aligned} \tag{4.46}$$

For the left-hand side of (4.46), we have

$$\begin{aligned} & \Big|\sum_{i=0}^{J}\sum_{j=i+1}^{J}(u_i,v_j)_A\Big| \\ \le\; & \Big|\sum_{i=0}^{N}\sum_{j=i+1}^{N}(u_i,v_j)_A\Big|+\Big|\sum_{i=0}^{N}\sum_{j=N+1}^{J}(u_i,v_j)_A\Big|+\Big|\sum_{i=N+1}^{J}\sum_{j=i+1}^{J}(u_i,v_j)_A\Big| \\ \triangleq\; & I_1+I_2+I_3. \end{aligned}$$

The estimates for I_1, I_2 and I_3 are given separately below.

• The estimation of I_1.

Lemma 4.16. *For any $\tau\in\overline{\mathscr{T}}_k$, $\bar{u}_k\in\overline{\mathbb{V}}_k(\tau)$, and $\bar{v}_l\in\overline{\mathbb{V}}_l(\tau)$ with $l\ge k$, there exists a constant $\gamma\in(0,1)$ such that $(\bar{u}_k,\bar{v}_l)_{A,\tau}\lesssim\frac{\lambda+\mu}{\sqrt{\mu}}\gamma^{l-k}\|\bar{u}_k\|_{A,\tau}\bar{h}_l^{-1}\|\bar{v}_l\|_{0,\tau}$.*

Lemma 4.17. *[5] For any $\gamma\in(0,1)$, it holds that $\sum_{l=0}^{L}\sum_{k=0}^{L}\gamma^{|k-l|}x_ky_l\lesssim(\sum_{k=0}^{L}x_k^2)^{1/2}(\sum_{k=0}^{L}y_k^2)^{1/2}$.*

The following theorem provides an estimate for I_1.

Theorem 4.18. *For any $u_i,v_i\in\mathbb{V}_i$ $(i=0,\cdots,N)$, the following holds*

$$\Big|\sum_{i=0}^{N}\sum_{j=i+1}^{N}(u_i,v_j)_A\Big|\lesssim\frac{\lambda+\mu}{\mu}\Big(\sum_{i=0}^{N}\|u_i\|^2_{A,\tilde{\omega}_i}\Big)^{1/2}\Big(\sum_{j=0}^{N}\|v_j\|^2_{A,\tilde{\omega}_j}\Big)^{1/2}. \tag{4.47}$$

Proof. The proof of (4.47) is presented in three steps.

Step 1. For any fixed $i, i=1(1)N$, we define

$$n(i)=\{j: j>i,\tilde{\omega}_j\cap\tilde{\omega}_i\neq\emptyset\} \tag{4.48}$$

and

$$w_k^i=\sum_{j\in n(i),g_j=k}v_j, \tag{4.49}$$

where $k\ge 1$ is an integer. For any $\tau\in\tilde{\omega}_i$, applying Lemma 4.5 and Lemma 4.16, we conclude that there exists a positive integer g_0 depending only on the shape regularity of the initial mesh $\mathscr{T}_0$, such that $u_i\in\overline{\mathbb{V}}_{g_i+g_0}$, and $w_k^i\in\overline{\mathbb{V}}_{k+g_0}$, and satisfies

$$(u_i,w_k^i)_{A,\tau}\lesssim\frac{\lambda+\mu}{\sqrt{\mu}}\gamma^{k-g_i}\|u_i\|_{A,\tau}\bar{h}_k^{-1}\|w_k^i\|_\tau. \tag{4.50}$$

Summing (4.50) over all elements τ in $\tilde{\omega}_i$, and applying the Cauchy-Schwarz inequality, the definitions of $|\cdot|_{A,\tilde{\omega}_i}$ and w_k^i, along with Lemma 4.6, we obtain

$$\begin{aligned}(u_i, w_k^i)_{A,\tilde{\omega}_i} &\lesssim \frac{\lambda+\mu}{\sqrt{\mu}}\gamma^{k-g_i}\sum_{\tau\in\tilde{\omega}_i}\|u_i\|_{A,\tau}\bar{h}_k^{-1}\|w_k^i\|_\tau \\ &\leq \frac{\lambda+\mu}{\sqrt{\mu}}\gamma^{k-g_i}\Big(\sum_{\tau\in\tilde{\omega}_i}\|u_i\|_{A,\tau}^2\Big)^{1/2}\bar{h}_k^{-1}\Big(\sum_{\tau\in\tilde{\omega}_i}\|w_k^i\|_\tau^2\Big)^{1/2} \\ &\leq \frac{\lambda+\mu}{\sqrt{\mu}}\gamma^{k-g_i}\|u_i\|_{A,\tilde{\omega}_i}\bar{h}_k^{-1}\Big(\sum_{g_j=k}\|v_j\|_{\tilde{\omega}_i}^2\Big)^{1/2},\end{aligned} \tag{4.51}$$

Step 2. For any given $u_i\in\mathbb{V}_i$ and $v_j\in\mathbb{V}_j$, $j=i+1(1)N$, using (4.48), (4.49), and (4.51), we have

$$\Big|(u_i,\sum_{j=i+1}^N v_j)_A\Big| \lesssim \frac{\lambda+\mu}{\sqrt{\mu}}\sum_{k=(g_i-g_0)^+}^L\Big(\gamma^{k-g_i}\bar{h}_k^{-1}\|u_i\|_{A,\tilde{\omega}_i}\Big(\sum_{g_j=k}\|v_j\|_{\tilde{\omega}_i}^2\Big)^{1/2}\Big). \tag{4.52}$$

Step 3. Let $\bar{C}=\frac{\lambda+\mu}{\sqrt{\mu}}$. Summing over u_i with index value l in (4.52), and applying the Cauchy-Schwarz inequality, (4.28), and the compact support property of v_j, we obtain

$$\begin{aligned}&\sum_{g_i=l}\Big|(u_i,\sum_{j=i+1}^N v_j)_A\Big| \\ &\lesssim \bar{C}\sum_{g_i=l}\sum_{k=(l-g_0)^+}^L\gamma^{k-l}\|u_i\|_{A,\tilde{\omega}_i}\bar{h}_k^{-1}\Big(\sum_{g_j=k}\|v_j\|_{\tilde{\omega}_i}^2\Big)^{1/2} \\ &= \bar{C}\sum_{k=(l-g_0)^+}^L\gamma^{k-l}\Big(\sum_{g_i=l}\|u_i\|_{A,\tilde{\omega}_i}^2\Big)^{1/2}\Big(\bar{h}_k^{-2}\sum_{g_j=k}\|v_j\|_{\tilde{\omega}_j}^2\Big)^{1/2}.\end{aligned} \tag{4.53}$$

By applying (4.53), Lemma 4.17, and (2.8), we obtain

$$\begin{aligned}&\sum_{l=0}^L\sum_{g_i=l}\Big|(u_i,\sum_{j=i+1}^N v_j)_A\Big| \\ &\lesssim \bar{C}\sum_{l=0}^L\sum_{k=0}^L\gamma^{|k-l|}\Big(\sum_{g_i=l}\|u_i\|_{A,\tilde{\omega}_i}^2\Big)^{1/2}\Big(\bar{h}_k^{-2}\sum_{g_j=k}\|v_j\|_{\tilde{\omega}_j}^2\Big)^{1/2} \\ &\lesssim \bar{C}\Big(\sum_{l=0}^L\sum_{g_i=l}\|u_i\|_{A,\tilde{\omega}_i}^2\Big)^{1/2}\Big(\sum_{k=0}^L\bar{h}_k^{-2}\sum_{g_j=k}\|v_j\|_{\tilde{\omega}_j}^2\Big)^{1/2} \\ &\lesssim \bar{C}\Big(\sum_{i=0}^N\|u_i\|_{A,\tilde{\omega}_i}^2\Big)^{1/2}\Big(\sum_{j=0}^N\|v_j\|_{1,\tilde{\omega}_j}^2\Big)^{1/2} \\ &= \frac{\lambda+\mu}{\mu}\Big(\sum_{i=0}^N\|u_i\|_{A,\tilde{\omega}_i}^2\Big)^{1/2}\Big(\sum_{j=0}^N\|v_j\|_{A,\tilde{\omega}_j}^2\Big)^{1/2}.\end{aligned} \tag{4.54}$$

From (4.54) and $\sum_{i=0}^N=\sum_{l=0}^L\sum_{g_i=l}$, we establish the validity of (4.47). □

• The estimation of I_2.

Theorem 4.19. *For any $u_i \in \mathbb{V}_i$ $(i = 0(1)N)$ and $v_j \in \mathbb{V}_j$ $(j = N+1(1)J)$, the following holds*

$$\Big|\sum_{i=0}^{N}\sum_{j=N+1}^{J}(u_i, v_j)_A\Big| \lesssim \sqrt{\lambda/\mu+1}\Big(\sum_{i=0}^{N}\|u_i\|^2_{A,\tilde{\omega}_i}\Big)^{1/2}\Big(\sum_{j=N+1}^{J}\|v_j\|^2_{A,\bar{\omega}_j}\Big)^{1/2}. \tag{4.55}$$

Proof. For any $u_i \in \mathbb{V}_i$ $(i = 0(1)N)$, by applying (4.47) and the compact support property of u_i, we have

$$\begin{aligned}\|\sum_{i=0}^{N}u_i\|^2_{A,\Omega} &\lesssim \sum_{i=0}^{N}\|u_i\|^2_{A,\Omega} + \frac{\lambda+\mu}{\mu}\sum_{i=0}^{N}\|u_i\|^2_{A,\tilde{\omega}_i} \\ &\lesssim \frac{\lambda+\mu}{\mu}\sum_{i=0}^{N}\|u_i\|^2_{A,\tilde{\omega}_i}. \end{aligned}\tag{4.56}$$

By employing (4.56), the Cauchy-Schwarz inequality, and the compact support property of v_j, we obtain

$$\begin{aligned}\Big|\sum_{i=0}^{N}\sum_{j=N+1}^{J}(u_i, v_j)_A\Big| &= \sum_{j=N+1}^{J}\Big|(\sum_{i=0}^{N}u_i, v_j)_{A,\bar{\omega}_j}\Big| \\ &\le \Big(\sum_{j=N+1}^{J}\|\sum_{i=0}^{N}u_i\|^2_{A,\bar{\omega}_j}\Big)^{1/2}\Big(\sum_{j=N+1}^{J}\|v_j\|^2_{A,\bar{\omega}_j}\Big)^{1/2} \\ &\lesssim \sqrt{\lambda/\mu+1}\Big(\sum_{i=0}^{N}\|u_i\|^2_{A,\tilde{\omega}_i}\Big)^{1/2}\Big(\sum_{j=N+1}^{J}\|v_j\|^2_{A,\bar{\omega}_j}\Big)^{1/2},\end{aligned}$$

we thus complete the proof of (4.55). □

• The estimation of I_3.

Theorem 4.20. *For any $u_i \in \mathbb{V}_i$ $(i = N+1(1)J)$ and $v_j \in \mathbb{V}_j$ $(j = N+1(1)J)$, the following holds*

$$\Big|\sum_{i=N+1}^{J}\sum_{j=i+1}^{J}(u_i, v_j)_A\Big| \le \Big(\sum_{i=N+1}^{J}\|u_i\|^2_{A,\bar{\omega}_i}\Big)^{1/2}\Big(\sum_{j=N+1}^{J}\|v_j\|^2_{A,\bar{\omega}_j}\Big)^{1/2}. \tag{4.57}$$

Proof. By applying the Cauchy-Schwarz inequality and the compact support properties of u_i and v_j, we obtain

$$\begin{aligned}\Big|\sum_{i=N+1}^{J}\sum_{j=i+1}^{J}(u_i, v_j)_A\Big| &\le \sum_{i=N+1}^{J}\sum_{j\in M_i}\|u_i\|_{A,\bar{\omega}_i}\|v_j\|_{A,\bar{\omega}_i} \\ &\le \Big(\sum_{i=N+1}^{J}\|u_i\|^2_{A,\bar{\omega}_i}\Big)^{1/2}\Big(\sum_{i=N+1}^{J}\big(\sum_{j\in M_i}\|v_j\|_{A,\bar{\omega}_i}\big)^2\Big)^{1/2} \\ &\lesssim \Big(\sum_{i=N+1}^{J}\|u_i\|^2_{A,\bar{\omega}_i}\Big)^{1/2}\Big(\sum_{j=N+1}^{J}\|v_j\|^2_{A,\bar{\omega}_j}\Big)^{1/2}.\end{aligned}$$

□

By applying Theorem 4.18, Theorem 4.19, and Theorem 4.20, and noting that $\frac{\lambda+\mu}{\mu} = \frac{1}{1-2\nu}$, we obtain the validity of condition **(P2)**, where

$$K_1 \lesssim \frac{1}{1-2\nu}, \tag{4.58}$$

and K_1 is a positive constant depending only on the Poisson's ratio ν. From (4.38), (4.58), and (4.17), we conclude that the convergence rate $\rho = 1 - \frac{1}{1+c_0} \in (0,1)$ of the LMG Algorithm 4.8 is a constant depending solely on the Poisson's ratio ν.

We now validate the theoretical results through numerical experiments.

5. Numerical Experiment and Result Analysis

In this section, one typical numerical example is presented to verify the convergence and quasi-optimal computational complexity of the aforementioned adaptive p-th order finite element method, as well as the computational efficiency and robustness of the LMG method for solving p-th order finite element equations on three-dimensional adaptive meshes. In all numerical experiments, the control tolerance tol in Algorithm 2.1 is set to 10^{-10}, $\bar{N}_{itr}$ denotes the number of iterations of the LMG method, and N_{dof} represents the total number of degrees of freedom.

Let $\Omega = (-1,1)^3 \setminus (0,1) \times (0,1) \times (0,1)$, the proper vector function f and the boundary g be chosen to ensure $u = (u_1, u_2, u_3)$ to be the solution of model (2.1)-(2.2), where

$$u_1 = \frac{1}{x^2+y^2+z^2+0.01},\ u_2 = x^2\cos(\pi y)\cos(\pi z),\ u_3 = y^2\cos(\pi x)\cos(\pi z).$$

The elastic modulus is set to $E = 3000$, and the Poisson's ratio is $\nu = 0.3$. The initial mesh used in the numerical experiments is shown in Figure 8.

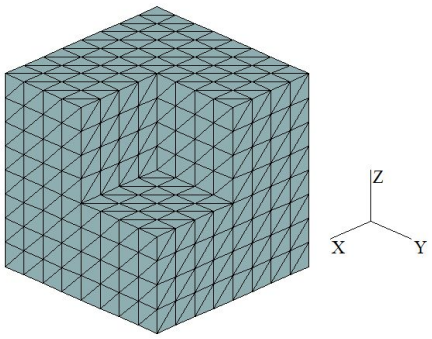

FIGURE 8. The initial mesh

Figure 9 and Figure 10 present the error curves for linear and quadratic elements, respectively, under different values of θ. To demonstrate the superiority of the adaptive finite element algorithm proposed in this paper, the error reduction results under uniformly refined meshes are also listed in the tables.

Table 1 shows the number of iterations for the LMG method when solving linear element equations on adaptive meshes with the Dörfler parameter $\theta = 0.5$. Table 2 provides the iteration counts for the LMG method when solving hierarchical quadratic element equations on adaptive meshes with $\theta = 0.5$.

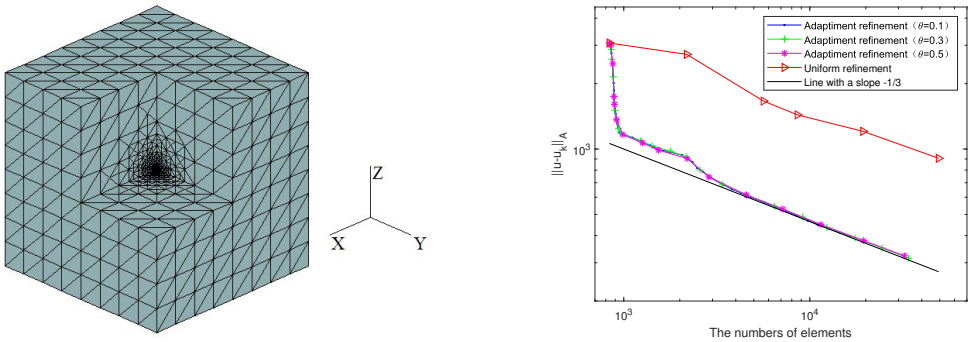

FIGURE 9. The refinement mesh $\mathscr{T}_{14}$ for $\theta = 0.5$(left) and the error curve for $\theta = 0.1, 0.3, 0.5$ (right) by linear finite element method.

J	3	5	7	9	11	13	15
N_{dof}	885	915	1260	2193	4569	11490	32316
$\bar{N}_{itr}$	18	18	32	36	39	49	45

TABLE 1. Iterative times for solving linear finite element equations under adaptive mesh by LMG method with $\theta = 0.5$.

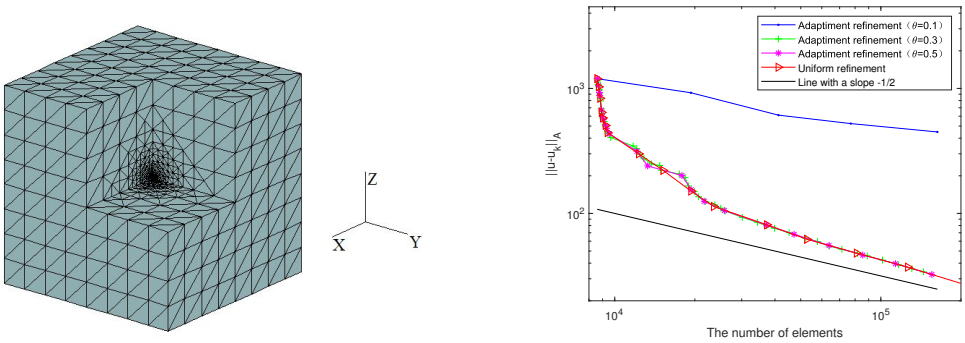

FIGURE 10. The refinement mesh $\mathscr{T}_{14}$ for $\theta = 0.5$(left) and the error curve for $\theta = 0.1, 0.3, 0.5$ (right) by quadratic finite element method

J	3	5	7	9	11	13	15
N_{dof}	8928	9231	12315	19359	37314	81087	208113
$\bar{N}_{itr}$	58	58	57	60	71	65	68

TABLE 2. Iterative times for solving quadrtic finite element equations under adaptive mesh by LMG method with $\theta = 0.5$.

The numerical results demonstrate that the proposed adaptive finite element method is convergent. For linear elements, the error curve decreases with increasing number of elements while maintaining parallelism to the reference line with a slope of $-\frac{1}{3}$, indicating quasi-optimal computational complexity. For quadratic elements, the error curve declines as the element count grows and runs parallel to the reference line with a slope of $-\frac{1}{2}$, achieving optimal computational accuracy with minimal effort. Furthermore, the LMG method proves highly efficient and

robust in solving both linear and hierarchical quadratic element equations on adaptively refined meshes. Notably, its iteration count remains nearly independent of both problem size and the number of adaptive refinement steps J.

6. CONCLUSIONS

The adaptive finite element method serves as an efficient numerical approach for solving three-dimensional stress concentration problems. It automatically performs mesh refinement in high-error regions by utilizing solution information from the current mesh, thereby achieving maximum computational accuracy with minimal computational effort. For the sequence of nested meshes generated through the adaptive process, the multigrid method can fully exploit its advantages of rapid convergence and high efficiency when solving the corresponding finite element equations. In this work, we proposed an improved LMG method with enhanced computational efficiency and robustness. This is achieved by decomposing the p-th order finite element space into "high-frequency" components and linear element spaces, while effectively incorporating the characteristics of mesh refinement. Although our numerical experiments are currently limited to cases where $p = 1$ and 2, the obtained results are nevertheless quite promising. Further research should focus on more extensive numerical testing for general practical problems, along with corresponding theoretical analysis of the algorithm. This includes investigating the quasi-optimal computational complexity of the adaptive algorithm and conducting convergence analysis for the LMG method.

Acknowledgements
The author was support by the Natural Science Foundation of Hunan Province (No. 2024JJ7203) and the key Project of Hunan provincial Education Department(No. 23A0577).

REFERENCES

[1] F. Bornemann and H. Yserentant, A basic norm equivalence for the theory of multilevel methods, Numerische Mathematik, 64 (1993) 455-476.
[2] Z. Cai, J. Korsaweand and G. Starke, An adaptive least squares mixed finite element method for the stress displacement formulation of linear elasticity, Numerical Methods for Partial Differential Equations, 21 (2005) 132-148.
[3] C. Carstensen, G. Dolzmann, S.A. Funken and D.S. Helm, Locking-free adaptive mixed finite element methods in linear elasticity, Computer Methods in Applie Mechanics and Engineering, 190 (2000) 1701-1718.
[4] J. Cascon, C.Kreuzer, R.H. Nochetto, and K. Siebert. Quasi-optimal convergence rate for an adaptive finite element method, SIAM Journal on Numerical Analysis, 46 (2008) 2524-2550.
[5] L. Chen, R.H. Nochetto and J. Xu, Optimal multilevel methods for graded bisection grids, Numerische Mathematik, 120 (2012) 1-34.
[6] P.G. Ciarlet, The Finite Element Method for Elliptic Problems, North-Holland, Amsterdam, 1978.
[7] R.A. Devore and G.G. Lorentz, Constructive Approximation, Spring-Verlag, New York, 1993.
[8] R. Hiptmair and W. Zheng, Local multigrid in $H(curl)$, Journal of Computational Mathematics, 27 (2009) 573-603.
[9] C. Liu, Y. Xiao, S. Shu, L. Zhong. Adaptive finite element method and local multigrid method for elasticity problems, Engineering Mechanics, 29 (2012) 60-67.
[10] C. Liu, L. Zhong, S. Shu and Y. Xiao, Convergence of an adaptive finite element method for 2D elasticity probles, Applied Mathmatics and Mechanics, 35 (2014) 969-978.
[11] Z. Meng, Y. Fang and Y. Cheng, A gast element-free Galerkin method for 3D elasticity problems, Computer Modeling in Engineering Sciences, 132 (2022) 55-79.

[12] W. Mitchell, Optimal multilevel iterative methods for adaptive grids, SIAM Journal on Scientific Computing, 13 (1992) 146-167.
[13] L.R. Scott and S. Zhang, Finite element interpolation of nonsmooth functions satisfying boundary conditions, Mathematics of Computation, 54 (1990) 483-493.
[14] Z. Tian, Y. Chen and J. Wang, A two-grid discretization method for nonlinear Schrödinger equation by mixed finite element methods, Computers & Mathematics with applications, 130 (2023) 10-20.
[15] R. Verfürth, A review of a posteriori error estimation techniques for elasticity problem, Computer Methods in Applie Mechanics and Engineering, 176 (1999) 419-440.
[16] J. Wang, A daptive refinement and multigrid solution for linear finite element method, Journal of Hohai University, 22 (1994) 16-22.
[17] H. Wu and Z. Chen, Uniform convergence of multigrid V-cycle on adaptively refined finite element meshes for second order elliptic problems, Science in China Series A-Mathematics Physics Astronomy, 49 (2006) 1405-1429.
[18] J. Wang, J. Jin and Z. Tian, Two-Grid finite element method with Crank-Nicolson fully discrete scheme for the time-dependent Schrodinger equation, Numerical Mathematics-Theory Methods and Applications, 13 (2020) 334-352.
[19] J.C. Xu and L. Zikatanov, The method of alternating projections and the method of subspace corrections in Hilbert space, Journal of the American Mathematical Society, 15 (2002) 573-597.
[20] L. Zhou and H. Xu, Local MG method for solving three-dimensional elasticity problems, Journal Nonlinear Functional Analysis, 2024 (2024) 1-17.